

Irradiation Microstructure of Austenitic Steels and Cast Steels Irradiated in the BOR-60 Reactor at 320°C

Yong Yang¹, Yiren Chen², Yina Huang³, Todd Allen³ and Appajosula Rao⁴

¹University of Florida, Gainesville, FL 32611, USA

²Argonne National Laboratory, Argonne, IL 60439, USA

³University of Wisconsin, Madison, WI 53706, USA

⁴US Nuclear Regulatory Commission, Washington, DC 20555 USA

Keywords: Neutron irradiation, BOR-60, PWR, and Dislocation loops

Abstract

Reactor internal components are subjected to neutron irradiation in light water reactors, and with the aging of nuclear power plants around the world, irradiation-induced material degradations are of concern for reactor internals. Irradiation-induced defects resulting from displacement damage are critical for understanding degradation in structural materials. In the present work, microstructural changes due to irradiation in austenitic stainless steels and cast steels were characterized using transmission electron microscopy. The specimens were irradiated in the BOR-60 reactor, a fast breeder reactor, up to ~40 dpa at ~320°C. The dose rate was approximately 9.4×10^{-7} dpa/s. Void swelling and irradiation defects were analyzed for these specimens. A high density of faulted loops dominated the irradiated-altered microstructures. Along with previous TEM results, a dose dependence of the defect structure was established at ~320°C.

Introduction

As many pressurized water reactors (PWRs) age and life extension of the aging plants is considered, high doses of neutron exposure and the associated property changes at the end of life (EOL) are anticipated. The PWR reentrant corners may be exposed up to 100 dpa at relatively high temperature due to gamma heating by EOL[1]. Several microstructural studies on PWR internal components have been reported in the literature [2-5], and the results indicate that the void swelling at 320-343°C is insignificant at doses to about 20 dpa. Nevertheless, the available microstructural data from PWR internals are very limited due to the difficulties in obtaining large salvaged reactor components after high doses of neutron irradiation. A common strategy to derive such information is to extrapolate the more abundant data gained under liquid-metal, fast breeder reactor conditions pertinent to PWR EOL or life-extension conditions[6-8].

Most of the in-core components of PWRs are constructed with austenitic stainless steels, particularly AISI 304L SS for the baffle/barrel/former assemblies and AISI 316 SS for fasteners, split pins and other components. The baffles are irradiated to a dose rate ranging from about 10^{-10} to 10^{-8} dpa/s [9], which is generally one to three orders lower than that in a fast reactor. However a higher rate is needed to achieve anticipated doses in a PWR within an acceptable time for controlled irradiation experiments. Reports indicate that there are subtle variations in microstructure as a function of dose rate that occur over this range of dose rates and experimentally accumulated doses and these changes are relatively minor [10], but any conclusion has to be drawn with particular caution.

The present work characterizes the microstructures of the austenitic stainless steels and cast steels irradiated in the BOR-60 fast reactor under PWR relevant temperature to a dose of 40 dpa. The dose rate is $\sim 9.4 \times 10^{-7}$ dpa/s which is higher than the rate of 1.4×10^{-7} dpa/s for typical PWR core components.

Experimental

Irradiation

Neutron irradiations were carried out in the BOR-60 reactor, a sodium-cooled fast breeder reactor located in the Research Institute of Atomic Reactors (RIAR), Dimitrovgrad, Russia. The TEM disks were loaded in four perforated capsules and one helium-tight capsule, as shown in Figure 1. The dpa values shown in the figure were targeted irradiation doses and the examined specimens in this paper were loaded in tube AN40, and the disks were in direct contact with sodium coolant during irradiation. The experiment included eight irradiation sub-cycles and several maintenance shut-down periods and the irradiation experiment was conducted in the fifth row of the core of the BOR-60 reactor. Neutron fluence was monitored by five dosimeters loaded in the central channel of the irradiation rig and in baskets with the specimens. The analyses of dosimeters were carried out by RIAR after irradiation. The irradiation temperature was controlled by monitoring the inlet and outlet sodium temperatures, which were kept at ≈ 315 and 325°C , respectively. Mg-Zn eutectic thermal monitors were also placed among specimens in several baskets during irradiation. Post-irradiation examination of these thermal monitors indicated that the irradiation temperature of capsules was below 343°C at all times.

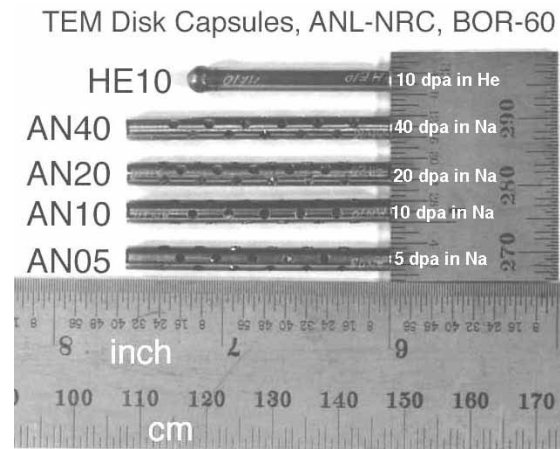


Figure 1. TEM capsules irradiated in the BOR-60 reactor (the dpa numbers in the figure are targeted irradiation doses).

Table I lists the chemical compositions of the examined alloys, the materials include austenitic stainless steels of 304 and 316, as well as cast steels with different carbon contents. The 304 solution annealed stainless steels include four variations with particularly tailored minor alloying elements. The two variations of 316 stainless steels contain low carbon and high nitrogen and one of them is doped with Titanium.

Table I. List of material type and associated chemical compositions of the disks irradiated in Bor-60 reactor for 40 dpa at 325 °C.

TEM Disk IDs	Material Type	Mater. Code	Composition (wt.%)								
			Ni	Si	P	S	Mn	C	N	Cr	Other Elements b
17	304 SA	B1	8.5	0.65	0.031	0.029	1.38	0.035	0.068	18.3	Mo 0.37
33	316 LN SA	B3	10.33	0.7	0.007	0.002	0.97	0.019	0.103	17.23	Mo 2.38, Cu 0.21
09	316 LN-Ti SA	B4	10.31	0.72	0.007	0.002	0.92	0.012	0.064	17.25	Mo 2.38, Ti 0.027, Cu 0.21
39	CF-3 cast SS	C1	9.4	0.92	0.012	0.005	0.57	0.009	0.052	19.49	Mo 0.35, δ 13.5%
48	CF-8 cast SS	C2	9.34	1.08	0.008	0.007	0.6	0.062	0.045	20.33	Mo 0.32, δ 13.5%
23	304 SA	A2	8.75	0.39	0.013	0.013	1.72	0.062	0.065	18.48	B <0.001
36	304 SA	A3	8.23	0.47	0.018	0.002	1	0.06	0.07	18.43	B <0.001
55	HP 304L SA	A8	9.03	0.03	<0.005	0.005	1.11	0.005	0.003	19.21	O 0.047, Mo <0.005

TEM Specimen Preparation

The TEM specimen preparation includes two steps, mechanical dimpling and subsequent electropolishing. The disks were mechanically dimpled from both sides before electropolishing for two purposes: one is to reduce the thickness of the specimens from ~400 μ m to the optimal thickness of ~150 μ m for electropolishing, and the other is to ensure the electro-perforation to be at the center of the specimen which can minimize the difficulty for locating the electron-transparent areas during TEM examination. A single-vertical-jet electropolisher from South Bay Technology Inc. (Model 550D) was used for electropolishing. The solution for stainless steel specimens contained 5% perchloric acid, 35% Butyl Cellosolve and 60% Methanol. The optimized polishing condition for SS was -20°C and 70mA current with a diaphragm in place. The height of jet nozzle was set at 3.5 mm from the assembly pedestal, and the flow rate was set at scale number 4 for all polishing.

TEM Examination

The TEM was performed using a JEOL 200CX TEM and the microstructural examination was focused on irradiation-induced defects, e.g. the Frank loops, voids or bubbles, and precipitations. General irradiation microstructure was imaged with a bright-field (BF) kinematical condition, where small dark spots can be seen in irradiated specimens. This imaging condition did not yield much detail information on irradiation defect due to complex initial microstructure of nonirradiated SSs. For a quantitative analysis of irradiation defects, relrod dark field (DF) imaging condition was used in this study. To reveal voids and bubbles, the through-focus technique was employed to introduce a phase-contrast component (Fresnel fringes) at high magnification. Because of the limitation of the microscope, small voids less than 1 nm were not readily resolved in this work.

Since the Frank loop is a major irradiation defect in fcc steels, the relrod DF technique can be applied. Irradiation-induced faulted dislocation loops have a Burgers vector of $a/3\{111\}$, and lie on $\{111\}$ planes in the austenitic structure. A relevant diffraction condition can be obtained by tilting the sample close to the $g = [311]$ two-beam condition near the zone axis $[011]$, and the relrod DF images were formed by selecting the relrod streak with the objective aperture. Figure 2 shows a schematic of relrod DF imaging condition. With the relrod DF images, size and density estimate of irradiation defects is much easier because initial nonirradiation microstructure is not present. One of the four variants of Frank loops can be observed in a single relrod picture. Assuming an isotropic distribution at all orientations, the density of Frank loops can be determined. The measurements were also performed near the perforation edge in regions that were less than 100-nm thick, which minimized the overlap of defects and improved the accuracy.

The thickness of the specimen was evaluated by tilting the specimen to 60° and measuring the projected perforation edge directly.

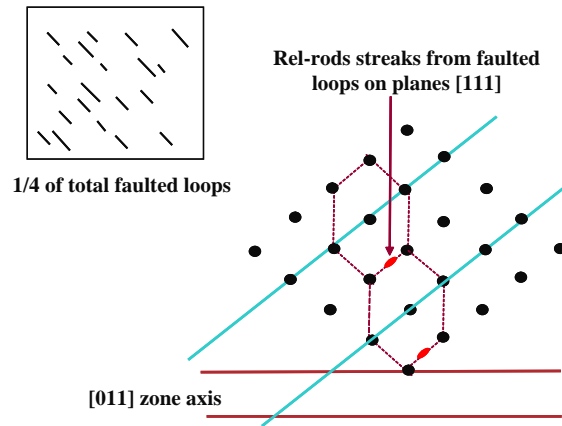
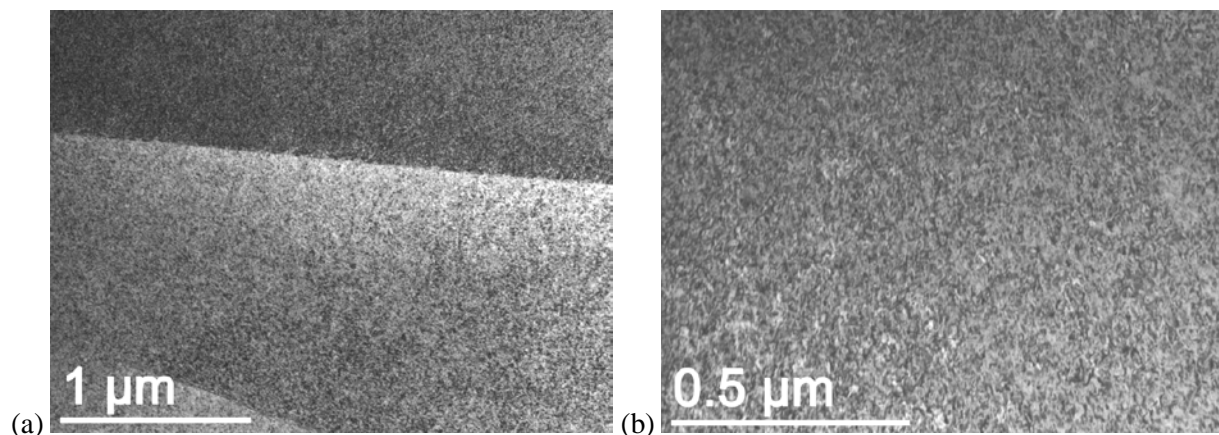


Figure 2. A schematic for relrod imaging condition.

Results and Discussion

304 Stainless Steels

The microstructures of irradiated 304 stainless steels are shown Figures 3-6. No voids were identified in any of these 304 SSs by checking the microstructures carefully at high magnification with a through-focus technique. Additionally no evidence of the existence of stacking fault tetrahedral was obtained. The specimen A2 shows the coexistence of the Frank loops and precipitates in Figure 2(b) and (c), while no significant precipitates were observed in the other three heats of 304 SS. No detectable connection could be found between the precipitates and the dislocation loops. The particles in heat A2 might precipitate synergistically from the relatively high contents of Mn and C. The irradiated microstructures of 304 SSs are dominated with a high density of dislocation loops as shown in the bright field images and relrod dark field images in Figures 3-6, respectively. The density of dislocation loops in 304 SSs are very close to each other, while the 304L SA have the largest average loop size and the 304 SA SSs (A2 and A3) has a very small loop size.



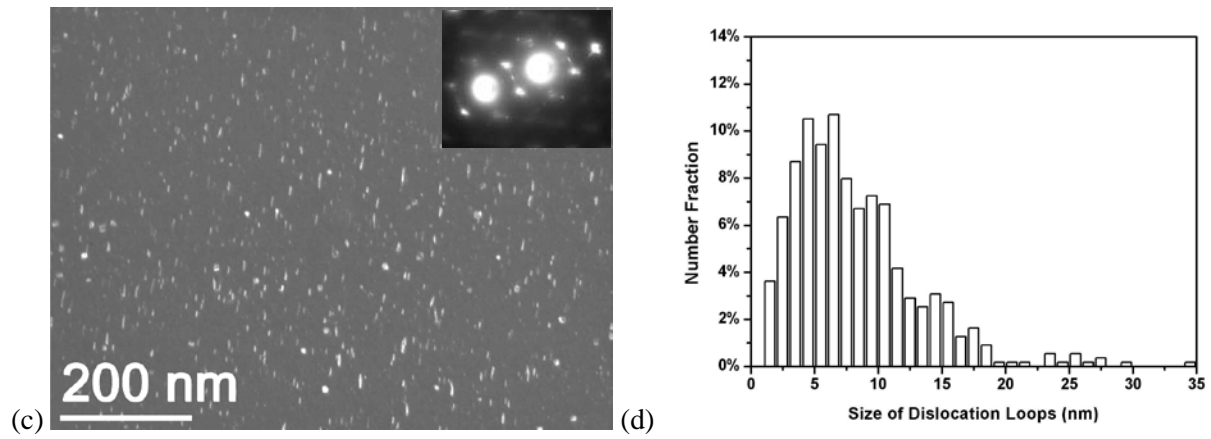


Figure 3. 304 SA-High S (A2). Micrographs were taken with the beam direction B close to $\langle 110 \rangle$: (a) general grain structures (b) bright field image (c) Relrod DF image of dislocation loops (d) size distribution of dislocation loops.

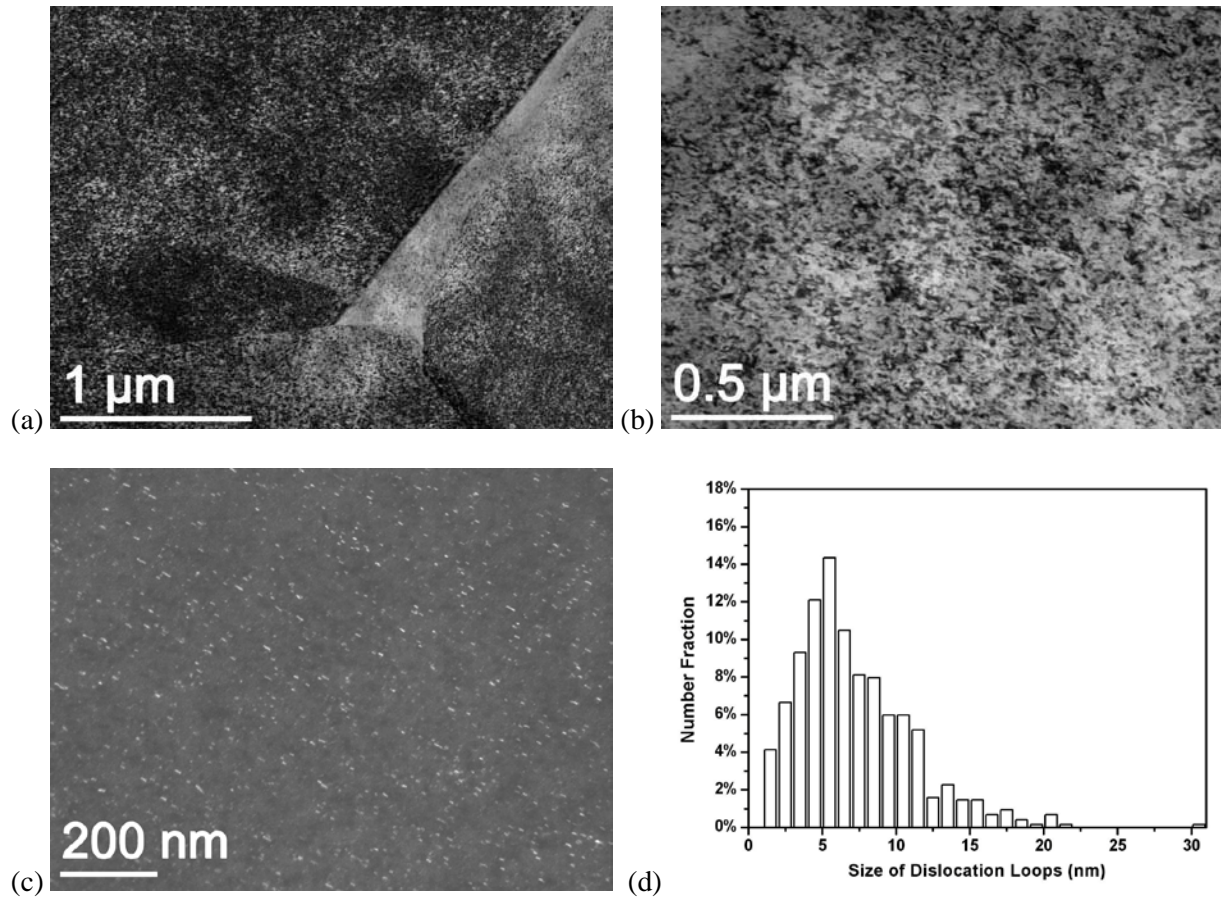


Figure 4. 304 SA-Low S (A3). Micrographs were taken with the beam direction B close to $\langle 110 \rangle$: (a) general grain structures (b) bright field image (c) Relrod DF image of dislocation loops (d) size distribution of dislocation loops.

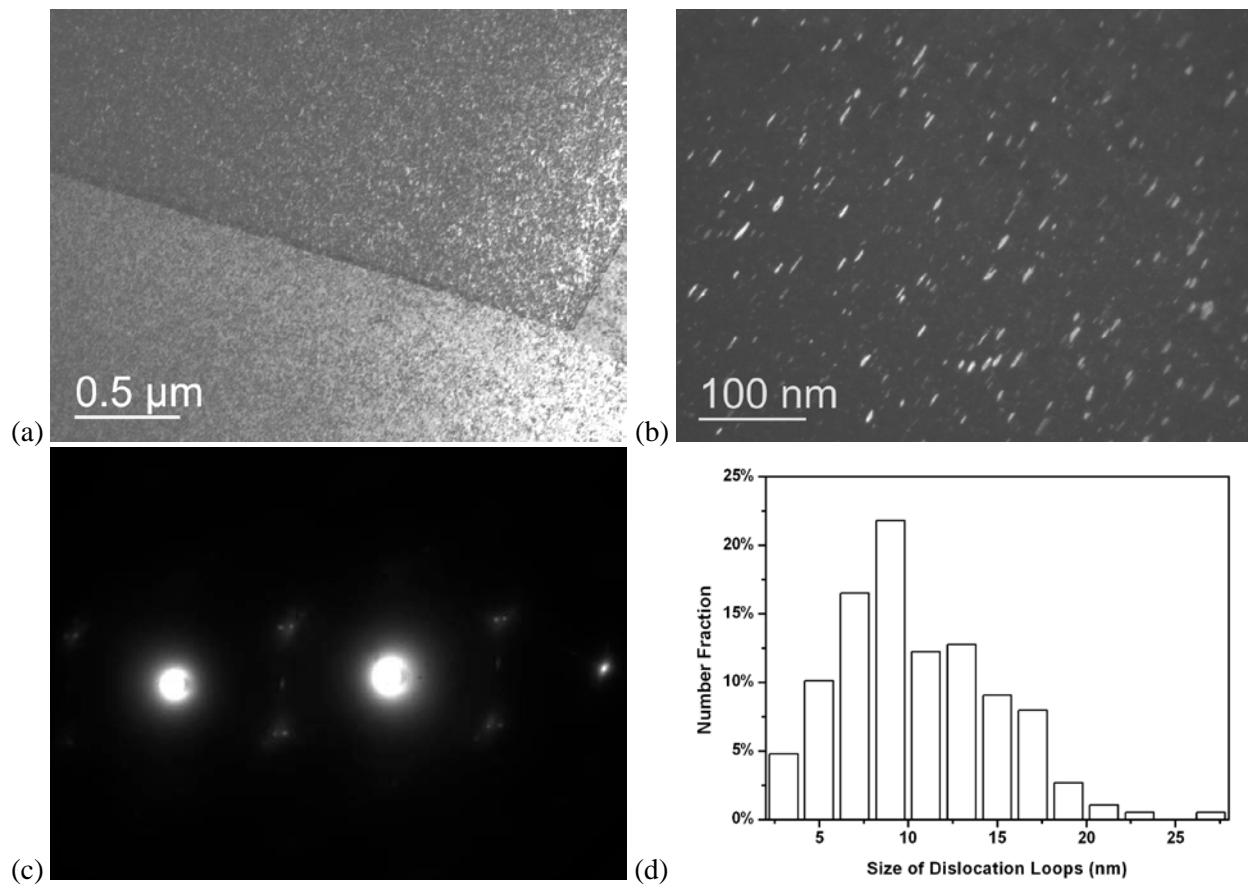
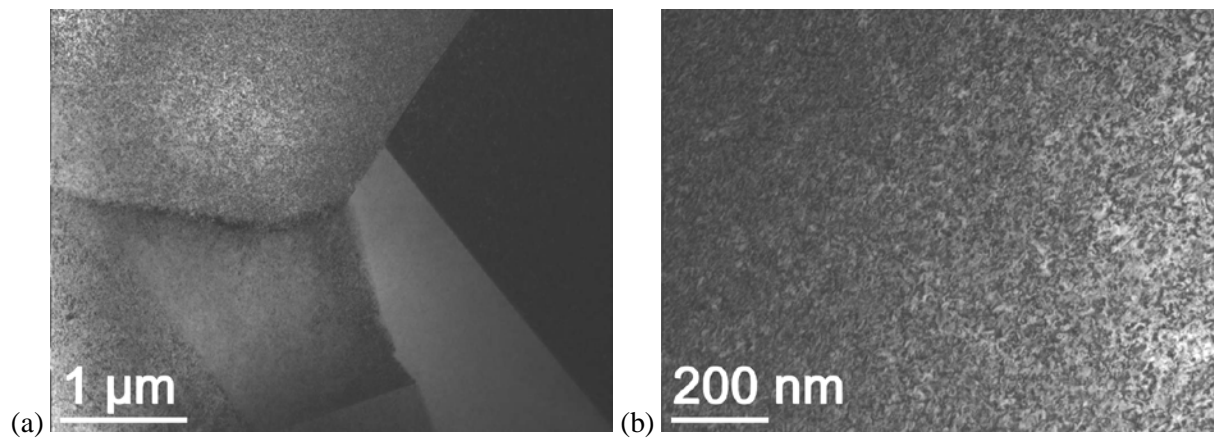


Figure 5. Microstructure of irradiated 304 SA (B1): (a) BF field image, (b) Relrod DF image of dislocation loops (c) Diffraction patterns showing the reflection streaks arising from dislocation loops, and (d) size distribution of dislocation loops.



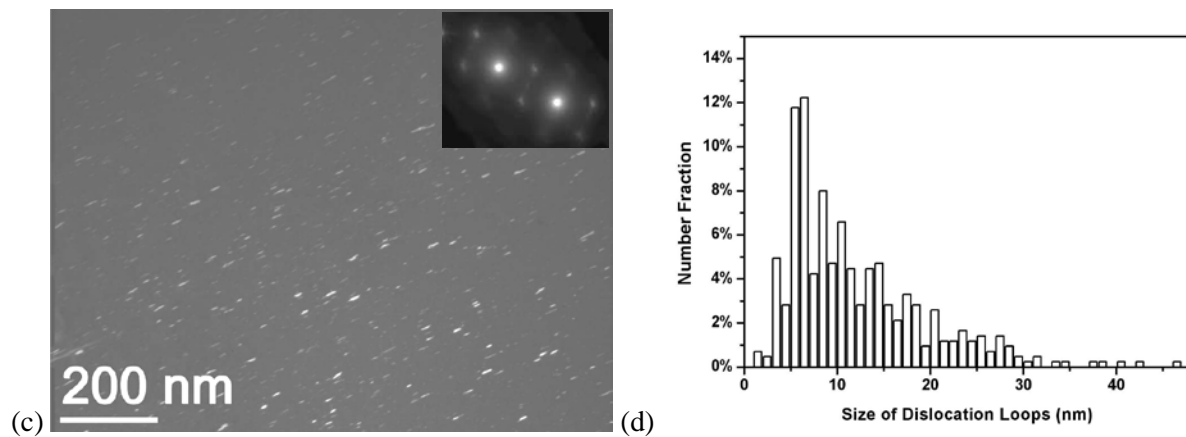
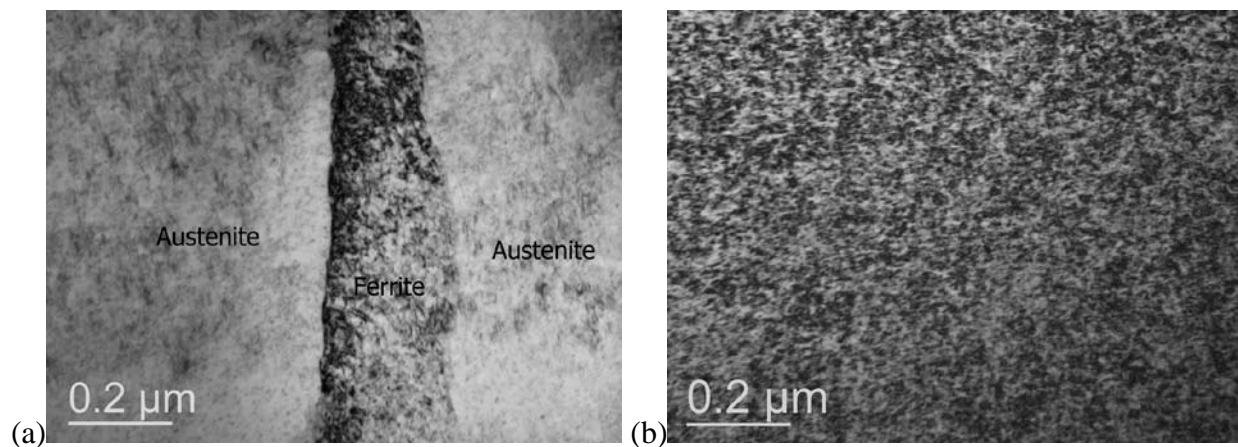


Figure 6. HP 304L SA (A8). Micrographs were taken with the beam direction B close to $\langle 110 \rangle$: (a) general grain structures (b) bright field image (c) Relrod DF image of dislocation loops (d) size distribution of dislocation loops.

Cast Steels

Figures 7 and 8 show the irradiated microstructures of the cast stainless steels (heat C1 and C2). As noted in Table I, heat C2 contains a much higher carbon content than heat C1 and they both have about 13.5% of δ ferrite phase existing as island bands among austenite phases. Similar to that in irradiated 304 SS, the irradiated microstructures feature a high density of dislocation loops, while no voids appear in either phase. Compared with austenite, the ferrite appears to have a lower density of dislocation loops. Both heats of C1 and C2 contain precipitates after irradiation, while the precipitates in C1 have a large average size but a much lower number density, as shown in Figure 7 (e). Irradiated heat C2 contains a high density of fine precipitates as shown in the dark field image of Figure 8 (c), and the diffraction pattern from both the austenite matrix and precipitates are shown in Figure 8 (d). The precipitate has a lattice parameter of $\sim 1.056\text{nm}$ which corresponds to $M_{23}X_6$ with a fcc crystal structure and the precipitates are coherent with the austenite matrix with orientation relationship of $[011]_{\gamma} \parallel [011]_{M_{23}X_6}$. The average size of fine $M_{23}X_6$ precipitates is about 6.7 nm and the number density is $7.3 \times 10^{21} \text{m}^{-3}$.



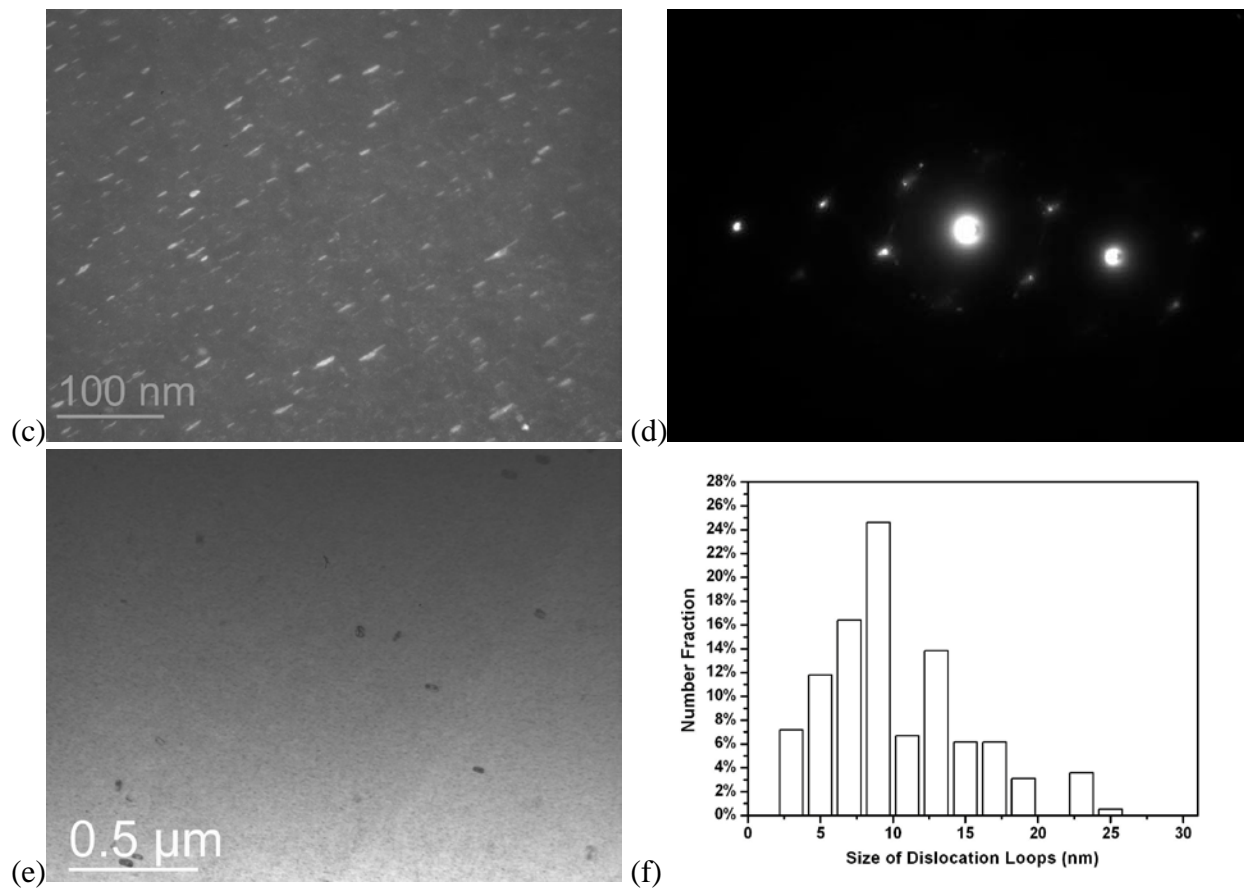
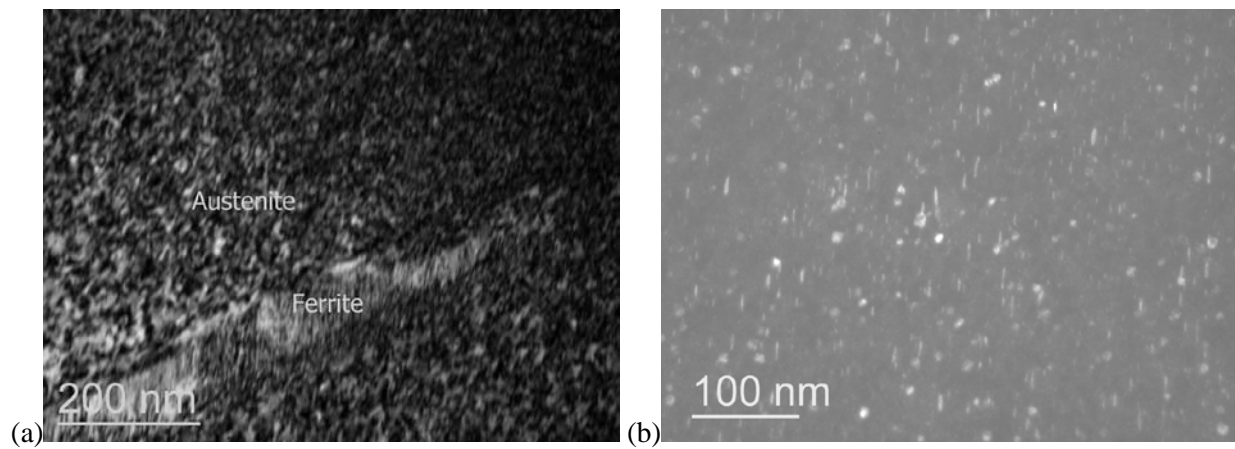


Figure 7. CF-3 cast SS (C1). Micrographs were taken with the beam direction close to $\langle 110 \rangle$: (a) BF field image of austenite and ferrite phases, (b) BF field of dislocation loops at low magnification, (c) Relrod DF image of dislocation loops, (d) Diffraction patterns showing the reflection streaks arising from dislocation loops, (e) precipitates in the austenite grain and (f) the size distribution of dislocation loops.



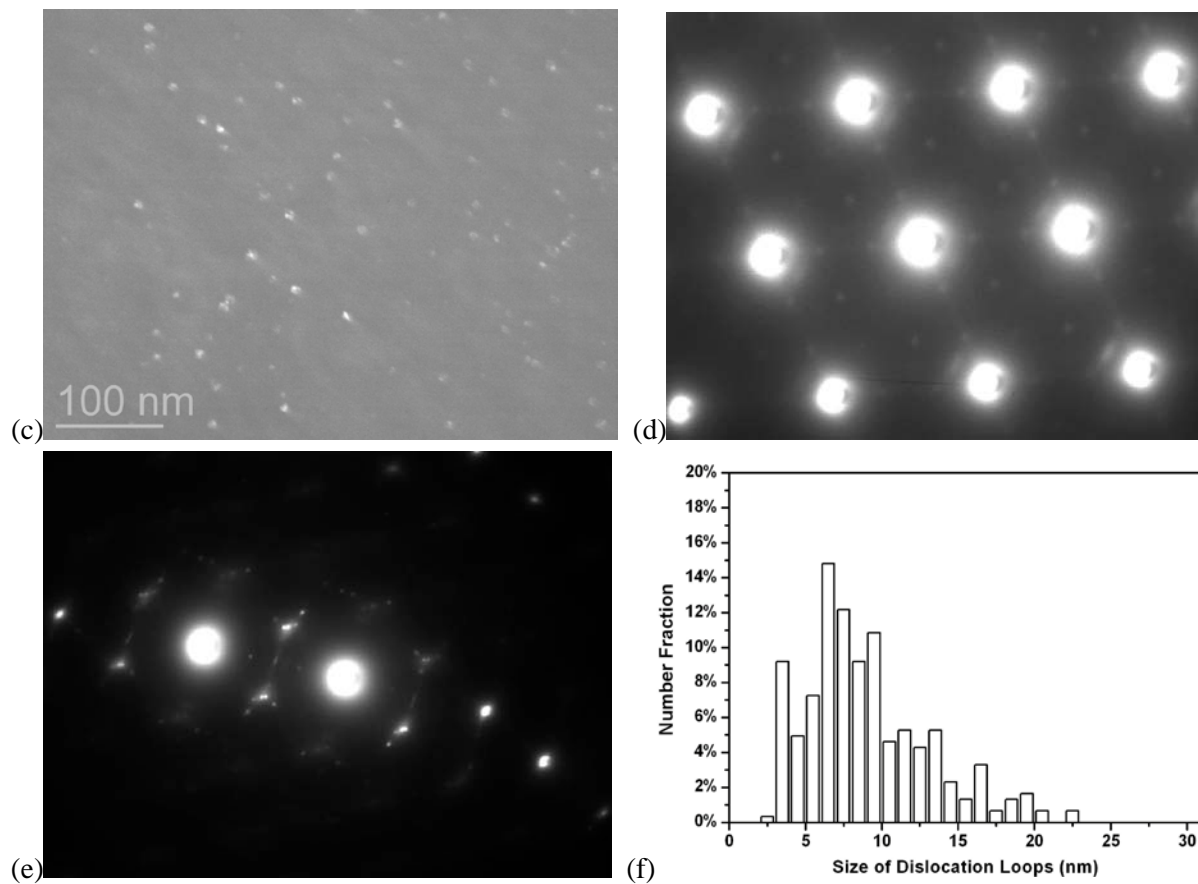


Figure 8. CF-8 cast SS (C2). Micrographs were taken with the beam direction B close to $\langle 110 \rangle$: (a) BF field image of austenite and ferrite phases, (b) Relrod DF image of dislocation loops, (c) Dark filed image of the fine precipitates in austenite grain using the ultra-reflections in (d), and (d) diffraction patterns showing the coherence of the precipitates with the matrix, (e) Diffraction patterns showing the reflection streaks arising from dislocation and (f) the size distribution of dislocation loops.

316 Stainless Steels

Figures 9-10 display the irradiated microstructure of 316 LN SA w/o Ti addition. Generally, no voids were observed in those two steels, and the irradiated microstructures are both decorated with a high density of dislocation loops. However, due to the complexity of the grain structure in the pristine materials, the size and number density of the dislocation loops were not quantified. Compared with the 316 LN SA, the irradiated 316 LN-Ti SA appears to have a moderate density of precipitates as shown in Figure 10 (b).

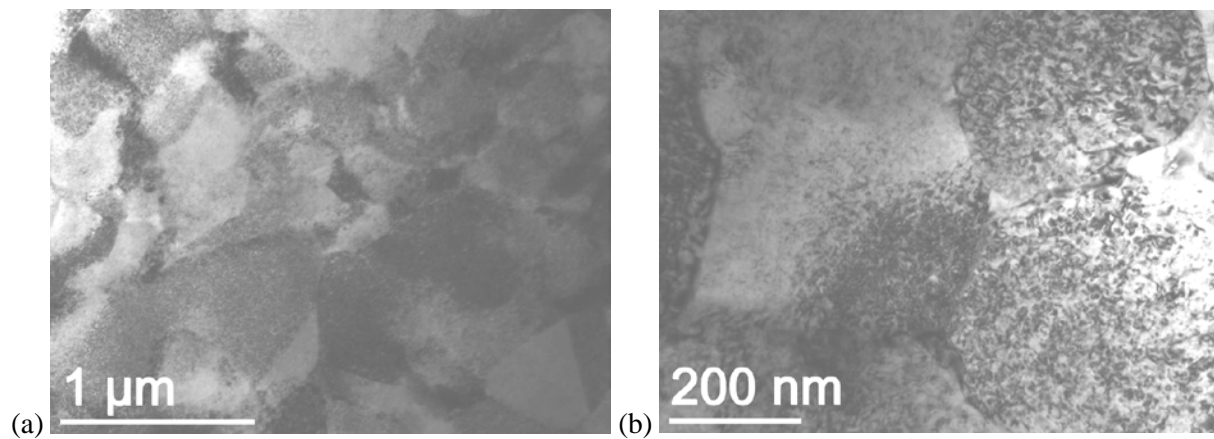


Figure 9. 316 LN SA (a) general grain structures (b) irradiation induced dislocation loops structure.

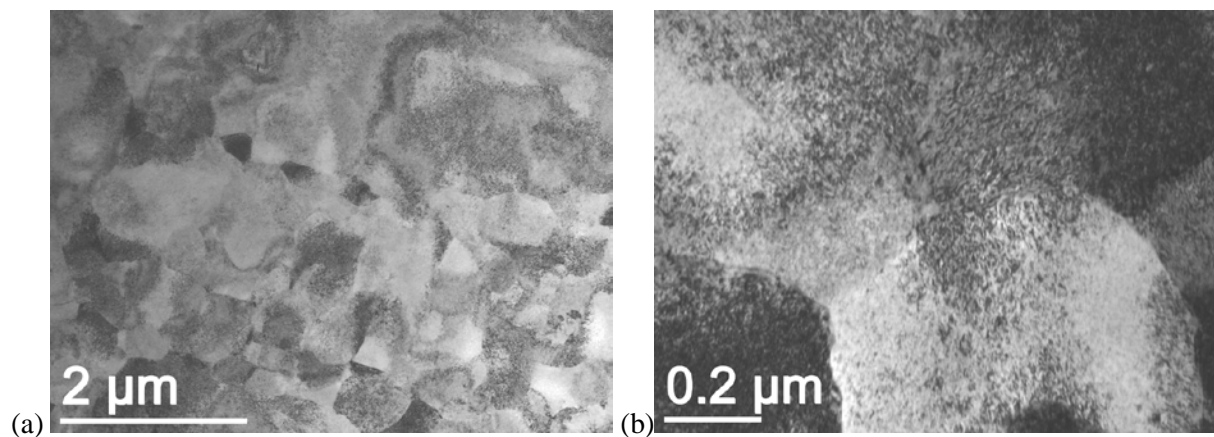


Figure 10. 316 LN-Ti SA (a) general grain structures (b) irradiation induced dislocation loops structure.

The irradiation induced microstructural features in the studied materials are listed in Table II. The cast steel CF-8, frequently used in the main coolant pipes of PWRs, has the highest density of dislocation loops and fine precipitates, and these austenite/ferrite duplex steels has mixed characteristics. Since no voids were observed, there is no clear relation between the swelling and the fine precipitates. HP304L SA contains the largest dislocation loop size while the density of the dislocation loops is close to those in other irradiated 304 SS variations. The evolution of the Frank loops in 304 SA-high S as a function of dose is given in Figure 11 by including our previous data at lower doses at the same irradiation temperature and dose rate [11]. The Frank loop density and size grow significantly with dose before 10 dpa, and at higher doses, a steady-state value is reached. No voids were observed in any examined materials, and the possible reason can be the synergic effects from the relatively high dose rate and low irradiation temperature. Our results are consistent with those from other investigators who examined 304 SA and 20%CW 316 w/o Ti addition irradiated to 5.4-25 dpa/320°C/ 9×10^{-7} dpa/s [10, 12].

Table II. Summary of Microstructural Characterization Results.

Material Type	Mat. Code	Frank loop Size (nm)	Frank Loop Density (m ⁻³)	Precipitate		Voids
				Density(m ⁻³)	Size (nm)	
304 SA-low S	A2	7.3	6.69×10^{22}	Dotted		Not observed
304 SA-high S	A3	7.8	5.8×10^{22}	Possible		Not observed
304 SA	B1	10.5	5.7×10^{22}	N/A		Not observed
HP 304L SA	A8	12.1	5.28×10^{22}	N/A		Not observed
CF-3 cast SS	C1	10.1	6.15×10^{22}	7.22×10^{19}	34	Not observed
CF-8 cast SS	C2	9.0	9.23×10^{22}	7.3×10^{21}	6.7	Not observed
316 LN SA	B3	Not quantified		Possible		Not observed
316 LN-Ti SA	B4			Dotted		Not observed

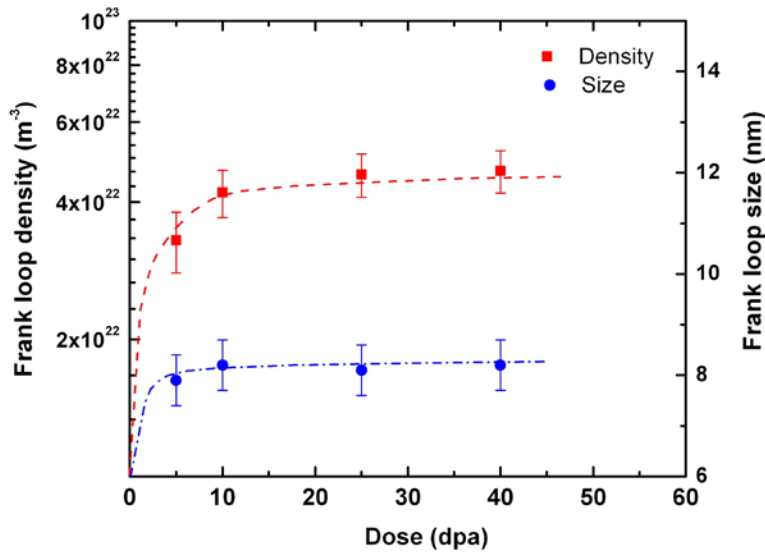


Figure 11. Density and size of Frank loops in irradiated 304 SA-High S.

Conclusion

TEM specimens of austenitic steels and cast steels irradiated to a dose of 40 dpa in the BOR-60 fast reactor at 320°C and 9.4×10^{-7} dpa/s have been studied by transmission electron microscopy. No voids were observed in any of these materials and the irradiated microstructures feature a high density of dislocation loops. The cast steel with a high content of carbon also contains a high density of nano-sized precipitates which were identified as coherent $M_{23}X_6$ particles. Based on the present results and the data from previously examined specimens at lower doses, the irradiated Frank loop density and size have already reached steady state after 10 dpa. Finally, the metallurgical state and the chemistry have a minimal effect on the dislocation loops but can directly affect the behavior of precipitation under irradiation.

Acknowledgement

This work is sponsored by the Office of Nuclear Regulatory Research, U.S. Nuclear Regulatory Commission, under Job Code N-6519. The opinions, findings, conclusions and recommendations expressed herein are those of the authors and do not necessary reflect the views of the NRC.

References:

1. Allen, T.R., et al. "Effects of Irradiation on the Swelling and Mechanical Properties of 316 Stainless Steel", *Proc. 11th Intl. Conf. on Environ. Degrad. of Mat. in Nucl. Power Syst.-Water React.* 2003. Stevenson, WA: NACE/ANS/TMS
2. S. Byrne, e.a. "Application of void swelling data to evaluation of pressurized water reactor components", *Proc. 10th Intl. Conf. on Environ. Degrad. of Mat. in Nucl. Power Syst.-Water React.* 2001. NACE/ANS/TMS
3. Garner, F.A., et al. "Generation and retention of helium and hydrogen in austenitic steels irradiated in a variety of LWR and test reactor spectral environments", *Proc. 10th Intl. Conf. on Environ. Degrad. of Mat. in Nucl. Power Syst.-Water Reactors.* 2001. NACE/ANS/TMS.127-147.
4. Edwards, D.J., et al. "Microstructural evaluation of a cold-worked 316 ss baffle bolt irradiated in a commercial PWR", *Proc. 10th Intl. Conf. on Environ. Degrad. of Mat. in Nucl. Power Syst.-Water React.* 2001. NACE/ANS/TMS
5. Fujii, K., et al. "Swelling in 316 stainless steel irradiated to 53 dpa in a PWR", *Proc. 10th Intl. Conf. on Environ. Degrad. of Mat. in Nucl. Power Syst.-Water React.* 2001. Houston, TX: NACE/ANS/TMS
6. Allen, T.R., et al., "Using Fast Reactor Component Evaluation for Pressurized Water Reactor Life Extension," *JOM*, October (1999), 27-32.
7. Garner, F.A., L.R. Greenwood, and D.L. Harrod. "Potential high fluence response of pressure vessel internals constructed from austenitic stainless steel", *6th Int. Symp. on Environ. Degrad. of Mat. in Nucl. Power Syst.-Water React.* 1993. San Diego, CA: TMS.783-798.
8. Foster, J.P., et al., "316 stainless steel cavity swelling in a PWR," *J. Nucl. Mater.*, 224 (1995), 207-315.
9. Maziasz, P.J., "Overview of Microstructural Evolution in Neutron-irradiated Austenitic Stainless Steels," *J. Nucl. Mater.*, 205 (1993), 118-145.
10. Edwards, D.J., et al. "Microstructural Evolution in Neutron-Irradiated Stainless Steels: Comparison of LWR and Fast-Reactor Irradiations", *12th Intl. Conf. Environ. Degrad. Mater. Nucle. Power Syst. Water React.* 2005. Salt Lake City, UT: TMS
11. Yang, Y., et al. "Dose Dependence of Radiation Hardening of Austenitic Steels in BOR-60 at PWR-Relevant Temperatures", *Proc. 10th Intl. Conf. on Environ. Degrad. of Mat. in Nucl. Power Syst.-Water React.* 2009. Virginia Beach, Virginia: ANS
12. Renault, A.E., et al. "Microstructure and Grain Boundary Chemistry Evolution In Austenitic Stainless Steels Irradiated in The BOR-60 Reactor Up to 120 DPA", *Proc. 14th Intl. Conf. on Environ. Degrad. of Mat. in Nucl. Power Syst.-Water React.* 2009. Virginia Beach, Virginia: ANS.1324-1334.